Solid-State NMR Analysis of $(GA)_3S(AG)_3D(GA)_3S(AG)_3D(GA)_3S(AG)_3$, a Peptide with a Lamellar Structure and a Calcium Binding Site, and Production of $TS[(AG)_3D(GA)_3S]_{16}$ in *Escherichia coli*

Tetsuo Asakura,*,† Hirohiko Sato,† Fumika Moro,† Mingying Yang,† Yasumoto Nakazawa,† Andrew M. Collins,‡ and David Knight§

Department of Biotechnology, Tokyo University of Agriculture and Technology, Koganei, Tokyo 184-8588, Japan, Department of Chemistry, Bristol University, Bristol BS8 1TS, U.K., and Oxford Biomaterials Ltd, Units 14-15 Galaxy House, New Greenham Business Park, RG19 6HR, U.K.

Received June 21, 2007; Revised Manuscript Received September 15, 2007

ABSTRACT: In an attempt to produce mineralized composite materials with potential use as biomaterials or scaffolds for tissue engineering, we designed silklike peptides based on Ala-Gly repeated sequences with a lamellar structure and Asp as a Ca binding site in the turn part as in Tirrell's work (for example: *Macromolecules* **1996**, *29*, 1540−1553). We further modified the design of the lamella structure by introducing a Ser residue between $(GlyAla)_3$ and $(AlaGly)_3$ sequences. At first, we synthesized three labeled versions of **41SDSDS**, $(GlyAla)_3Ser(AlaGly)_3Asp(GlyAla)_3Ser(AlaGly)_3Asp(GlyAla)_3Ser(AlaGly)_3$, with ^{13}C labeling in different positions to characterize the lamellar structure using ^{13}C CP/MAS and spin-diffusion solid-state NMR. The β-sheet fraction in Ala residues increased with increased distance from the Asp residue in the turn part. The introduced Ser residue took almost 100% β-sheet structure probably because it forms an extra hydrogen bond stabilizing the stem part of $(AlaGly)_n$. Thus, position-selective and sensitive information useful to characterize the detailed lamella structure with heterogeneous local conformations, can be obtained by ^{13}C selective labeling of the peptide and determining ^{13}C conformation-dependent NMR chemical shifts. We then produced an analogous recombinant protein, **14DS16**, $ThrSer[(AlaGly)_3Asp(GlyAla)_3Ser]_{16}$ in *Escherichia coli* as a possible biomaterial. Films of this protein treated with simulated body fluid were rapidly mineralized with hydroxyapatite.

Introduction

Bombyx mori silk fibroin is capable of being extruded into fibers with exceptional tensile properties.[1] These properties are thought to depend on the ability of this protein to fold into a structure largely composed (approximately 60%) of well ordered β-sheet crystals.[2,3] This imparts a wet strength and toughness to naturally spun *B. mori* silk considerably in excess of that of collagenous materials.[1] These considerations have prompted numerous investigations into the potential of fibroin in implantable biomaterials and scaffolds for tissue engineering.[4−12] Furthermore, collagen-based synthetic biomaterials for bone repair generally have poor compressive properties and are therefore limited to acting as carriers for osteoinductive factors for applications in which rapid load bearing is not required,[2] suggesting that silk-based materials may be stronger and tougher than collagen-based ones in bone repair.[5,9,10]

Marsh et al.[13] were the first to propose an antiparallel β-sheet structural model for native *B. mori* silk fiber based on a wide-angle X-ray scattering. Takahashi et al.[14] reported a more refined X-ray fiber diffraction analysis of *B. mori* silk fibroin. These authors proposed that silk II, the form present in the fiber, consists of antipolar antiparallel β-sheet structures, as proposed by Marsh et al., but statistically stacked together in two different ways with a ratio of 1:2 to form the crystals. For the structural analysis of *B. mori* silk fibroin, poly(alanylglycine) (poly(AG)) and alanine-glycine copolypeptides $(AG)_n$ have been used as models in spectroscopic studies.[13−17]

We found that the Ala Cβ peaks in the CP/MAS NMR spectra of both the *B. mori* silk fibroin fiber and in $(AG)_{15}$ in the silk II form are broad and asymmetric, reflecting a heterogeneous structure.[16,17] The relative proportions of the various heterogeneous components were determined from their relative peak intensities after line shape deconvolution. For example, the deconvolution of $(AG)_{15}$ gave 27% *distorted* β-turn (16.7 ppm); 46% β-sheet (alternating Ala residues)(19.9 ppm); and 27% β-sheet (parallel Ala residues)(22.1 ppm). Panitch et al.[18] produced $(AG)_{64}$ from recombinant *Escherichia coli*, and presented SANS and WAXS evidence for the chain-folded lamella structural model of this peptide in the silk II form. The structure consists of polar antiparallel β-sheets with repetitive folding through γ-turns from every eighth amino acid (including the fold), stacking with like surfaces together. In our recent papers,[19,20] using ^{13}C high-resolution solid-state NMR coupled with selective ^{13}C isotope-labeling of the Ala methyl groups, we showed that $(AG)_{15}$ in the silk II structure had the folded-lamella structure. This contained a combination of distorted β-turns with a large distribution of the torsion angles and antiparallel β-sheets. Namely, the fraction of the peak at 16.7 ppm in the Ala Cβ region increased appreciably at the positions 9 and 11, suggesting a folded lamellar structure with a β-turn at these positions and then the decreased fractions after the 11th position remain unchanged until the 17th position, and the fraction reached the next maximum at the 19th position again. These changes in the fraction of the peak at 16.7 ppm indicate the presence of lamellar structure. A statistical mechanical analysis of $(AG)_{15}$in the silk II state was in excellent agreement

* To whom correspondence should be addressed. E-mail: asakura@cc.tuat.ac.jp.
† Tokyo University of Agriculture and Technology.
‡ Bristol University.
§ Oxford Biomaterials Ltd.

10.1021/ma0713759 CCC: $37.00
Published on Web 11/07/2007

with this lamellar structure. The 2D spin diffusion ^{13}C solid-state NMR spectra of two doubly labeled peptides, [1-^{13}C]Gly^{14}-[1-^{13}C]Ala^{15}- and [1-^{13}C]Gly^{18} [1-^{13}C]Ala^{19}- of $(AG)_{15}$ and REDOR measurements of five kinds of atomic distances between doubly labeled ^{13}C and ^{15}N nuclei in five labeled versions of $(AG)_{15}$ were consistent with the lamellar structure containing a combination of antiparallel β-sheets and distorted β-turns with a large distribution of the torsion angles. Thus, these solid-state NMR analyses coupled with the preparation of selectively stable isotope labeled peptides are very powerful methods to analyze the lamella structure in detail.

For design and control of the molecular and supermolecular properties of polymeric systems, Tirrell et al.[21−23] have previously reported the biosynthesis of highly repetitive, monodisperse, artificial silklike protein analogs, including derivatives containing nonprotein amino acids or elastomeric domains. For example, they produced $\{(AlaGly)_3GluGly(GlyAla)_3GluGly)\}_{10}$ and poly$(AlaGly)_3$GluGly in *E. coli* by genetic engineering. The purified proteins were prepared as crystalline mats with formic acid through gel formation and the structures were analyzed mainly by detailed X-ray diffraction and solid state ^{13}C CP/MAS NMR methods. The X-ray diffraction patterns of these crystallized proteins were consistent with the folding periodicity in-phase with the amino acid sequence and with the γ-turns and the Glu residues confined to the lamella surfaces. Crystallization induced changes in the chemical shift of Cα carbon of the Glu residue, but the dynamic behavior of the Glu side chain carbons was unchanged. These NMR data indicate that this side chain is excluded from the crystalline region and supports the assignment of Glu to turn positions at the lamella surface. In the Ala Cβ carbon region of these proteins, the 16.8 ppm peak was assigned to reverse turn structures which is consistent with the X-ray diffraction results and IR and Raman analyses.[22]

In a previous attempt to produce novel mineralized biomaterials we introduced the calcium-binding site from the protein MSI60 found in the nacreous layer of pearl oyster, *Pinctada fucata*[24] into artificial silklike proteins.[25] This calcium binding site has an Asp rich sequence, EYDYDDDSDDDDEWDG and was introduced between Ala-Gly repeats derived from the primary sequences of several lepidopteran and spider silk fibroins. Ca^{2+} binding assays on these modified silklike peptides showed that the ability of the MSI60 domain to bind calcium was highest when the flanking silklike Ala-Gly sequences were in the β-sheet structure. This indicated that structural stability of flanking domains was important for calcium binding.

For the present paper we sought to produce novel biomaterials with potential as bone repair materials based on the work described above but using a simpler and improved approach to confer calcium binding. We designed two novel artificial silklike materials (**41SDSDS** and the much larger **14DS16)** both based on Ala-Gly repeated sequences with a lamellar structure, Asp as a Ca binding site in the turn part, and a Ser residue between $(GlyAla)_3$ and $(AlaGly)_3$ sequences to strengthen the stem part. We introduced a single Asp between the $(AG)_3$ and $(GA)_3$ hexapeptides with the intention that the flanking Gly residues would provide flexibility for a turn centered on this Asp. In addition we introduced a single Ser residue between $(GA)_3$ and $(AG)_3$ sequences as there is evidence that the presence of these residues stabilizes the β-sheet structure in *B. mori* silk fibroin in the silk II structure by hydrogen bonding between their side chain OH and backbone carbonyl groups.[26−28] The palindromic structure of the peptide was selected to provide for a systematic arrangement of the β-sheet and turn regions thus favoring an ordered lamellar structure (Figure 1). Palindromic regions with

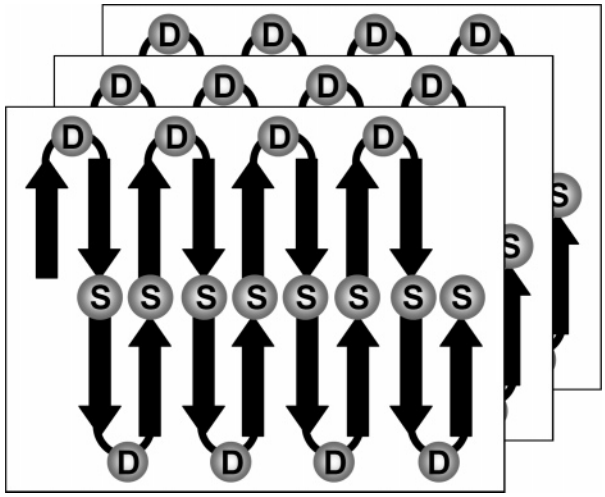

Figure 1. Design of lamellar structure of the silklike peptide based on Ala-Gly repeated sequences with antiparallel β-sheet structure, where Asp (D) is a Ca binding site in the turn part and a Ser (S) residue is located between $(GlyAla)_3$ and $(AlaGly)_3$ sequences to strengthen the stem part of the lamella.

systematically arranged Ser residues are indeed found in *B. mori* heavy chain fibroins.[28] This introduction of Ser is a novel approach in the design of synthetic silklike materials based on Ala-Gly repeated sequences with a lamellar structure. At first, in order to characterize the lamellar structure in detail, we observed ^{13}C CP/MAS NMR spectra of three ^{13}C doubly labeled versions of **41SDSDS**, $(GlyAla)_3Ser(AlaGly)_3$-Asp$(GlyAla)_3Ser$-$(AlaGly)_3Asp(GlyAla)_3Ser(AlaGly)_3$, and 2D spin diffusion ^{13}C solid-state NMR spectrum of the peptide labeled at two successive carbonyl carbons. We then produced a much larger analogue of this peptide, **14DS16**, ThrSer$[(AlaGly)_3Asp$-$(GlyAla)_3Ser]_{16}$ by overexpression in *E. coli* to examine the potentiality of this artificial protein with unique sequence for mineralization by hydroxyapatite.

Experimental Section

Peptide Preparations. For ^{13}C CP/MAS NMR we used solid-phase Fmoc-chemistry to prepare a non-labeled **41SDSDS**, and three versions of the same peptide with double labeling as follows: (a) [1-^{13}C]Ala^{12}-, [3-^{13}C]Ala^{16}-/(b) [1-^{13}C]Ala^{10}-, [3-^{13}C]Ala^{18}-/(c) [1-^{13}C]Ala^{8}-, [3-^{13}C]Ala^{20}- (see Table 1). For 2D spin diffusion ^{13}C solid-state NMR we prepared the same peptide doubly labeling as follows: (f) [1-^{13}C]Gly^{15}[1-^{13}C]Ala^{16}- (see Table 1). A fully automated Pioneer Peptide Synthesis System (Applied Biosystem Ltd.) was used throughout. After synthesis, these samples were dissolved in 9 M LiBr followed by dialysis against water and lyophilization and then dissolved in formic acid followed by precipitation in methanol and thoroughly dried before use in NMR experiments.[19,20] Our approach to the design of a lamellar structure is essentially the same as that reported by Wang et al.[22] for $\{(AlaGly)_3GluGly(GlyAla)_3Glu$-$Gly)\}_{10}$ and poly$(AlaGly)_3$GluGly but with the systematic introduction of Ser (see above).

^{13}C CP/MAS NMR Measurements. ^{13}C CP/MAS NMR experiments were performed on a Chemagnetics Infinity 400 MHz spectrometer with an operating frequency of 100.0 MHz for ^{13}C at a sample spinning rate of 8 kHz in a 4 mm diameter ZrO_2 rotor. A total of 16 300 scans for the nonlabeled sample and 4100−4300 scans for labeled samples were collected over a spectral width of 35 kHz with a recycle delay of 3 s. A 50 kHz radio frequency field strength was used for $^1H-^{13}C$ decoupling with the acquisition period of 12.8 ms. A 90° pulse width of 3.25 μs with 1 ms CP contact time was employed. Phase cycling was used to minimize artifacts. ^{13}C chemical shifts were calibrated indirectly using the adamantane methine peak observed at 28.8 ppm relative to TMS (tetramethylsilane) at 0 ppm.[16,17,19,20,29]

Table 1. Samples for CP/MAS NMR and 2D Spin Diffusion ^{13}C Solid-State NMR

sample	preparation	methods
(a) $(GA)_3S(AG)_2[1\text{-}^{13}C]A^{12}GDG[3\text{-}^{13}C]A^{16}(GA)_2S(AG)_3D(GA)_3S(AG)_3$	solid-phase synthesis	CP/MAS
(b) $(GA)_3SAG[1\text{-}^{13}C]A^{10}GAGDGAG[3\text{-}^{13}C]A^{18}GAS(AG)_3D(GA)_3S(AG)_3$	solid-phase synthesis	CP/MAS
(c) $(GA)_3S[1\text{-}^{13}C]A^{8}G(AG)_2D(GA)_2G[3\text{-}^{13}C]A^{20}S(AG)_3D(GA)_3S(AG)_3$	solid-phase synthesis	CP/MAS
(d) $(GA)_3S(AG)_3D(GA)_3S(AG)_3D(GA)_3S(AG)_3$	solid-phase synthesis	CP/MAS
(e) $TS[(AG)_3D(GA)_3S]_{16}$	*E. coli*	CP/MAS
(f) $(GA)_3S(AG)_3D[1\text{-}^{13}C]G^{15}[1\text{-}^{13}C]A^{16}(GA)_2S(AG)_3D(GA)_3S(AG)_3$	solid-phase synthesis	spin-diffusion

2D Spin Diffusion ^{13}C Solid-State NMR Measurements. The 2D spin-diffusion NMR spectrum was obtained using a Varian Unity *INOVA* 400 NMR spectrometer with a 7 mm Jakobsen-type double-tuned MAS probe at off magic angle condition ($\theta_m - 6.2°$) at room temperature.[30] The sample spinning rate was 5 kHz. The scaling factor of the 2D spin-diffusion spectra is $^1/_2(3\cos^2(\theta_m - 6.2°) - 1) = 0.158$. The mixing times were set to 2 s. The contact time was set to 1 ms using the variable-amplitude CP technique. The principal values of the chemical shift tensors for the carbonyl carbon nuclei of the ^{13}C-labeled Ala and Gly residues were determined by analysis of the spinning sidebands under slow MAS conditions using a Varian Unity *INOVA* 400 NMR spectrometer.[30]

Gene Construction and Protein Expression. The oligonucleotide fragment encoding the His-tagged **14DS16** was annealed by heating at 95 °C and cooling slowly to room temperature over about 3 h. The monomer was constructed by inserting the duplex DNA into the *SpeI* and *NheI*-digested pUC118-linker. The multimers were obtained using previously reported strategies involving head-to-tail ligation and orientation for *NheI* and *SpeI* sites.[31−33] Octamer DNA fragments were inserted into *BamH I and HindIII*-digested expression vector pET30a. The ligated mixture was used to transform the *E. coli* expression host strain BL21(DE3)pLysS. Protein expression, under control of a bacteriophage T7 promoter, was induced by addition of IPTG to a final concentration of 1 mM in Luria−Bertani broth containing chloramphenicol (25 uL/mL) and kanamycin (25 uL/mL) at 37 °C. His-tagged fusion proteins were purified on a nickel chelate affinity column under native conditions after charging the His tags with Ni^{+2}. The identity of the construct was confirmed by MALDI using an Applied Biosystems Voyager DE PRO. This showed a single high molecular weight peak at 24.1 kDa in agreement with the theoretical M_w of 23.8 kDa for the His-tagged construct. The final yield of the purified protein was about 20 mg/L of the medium.

Mineralization of the Cast Films. Cast films were prepared by dissolving the genetically engineered protein in formic acid followed by precipitation with methanol. Prior to mineralization, films were heated to 100 °C for 30 min to increase β-sheet structure. Calcification was performed by pretreating films in 200 mM $CaCl_2$ (pH 7.4) solution for 1 h at room temperature followed by soaking at room temperature in 1.5 strength simulated body fluid (SBF) solution buffer for up to 7days at 20 °C using a similar protocol to that described in a previous study.[34] After rinsing with distilled water and air drying, the surface of films were monitored with an SEM (VE-7800, KEYENCE). Films were observed after soaking in 1.5 SBF solution buffer for 1, 3, 5, and 7 days. For high-resolution SEM, films mounted on aluminum stubs using adhesive carbon pads were sputter coated with platinum to a thickness between 10 and 20 nm. Both a JEOL JSM 5600 SEM and a JEOL JSM 6330 FEG SEM were used. Samples were examined under high vacuum (10^{-4} mbar) and images were recorded digitally. For energy dispersive X-ray analysis (EDXA) both microscopes were fitted with an Oxford Instruments X-ray Analysis ISIS 300 with an atmospheric thin window for light element detection. EDXA was performed at an accelerating voltage of 20 KV and a working distance of 15 mm. For FT-IR, samples were pressed into discs with KBr using a hydraulic press prior to examination with a Perkin-Elmer Spectrum 1 spectrometer driven by Spectrum Analysis software. A Siemens D500 powder diffractometer with a Cu Kα radiation source ($\lambda = 0.15405$ nm) was used to demonstrate hydroxyapatite in the films. Samples were powdered before placing in a sample holder.

Results and Discussions

^{13}C CP/MAS NMR Spectra of 41SDSDS and 14DS16. Figure 2shows the ^{13}C CP/MAS NMR spectra of three ^{13}C doubly labeled versions of **41SDSDS** (a−c), nonlabeled version of the same peptide (d), and the nonlabeled silklike protein analogue **14DS16** produced in *E. coli* (e). The ^{13}C chemical shifts are summarized in Table 2. In general, the ^{13}C chemical shifts of the Cα and Cβ carbons in proteins and peptides exhibit conformation-dependent changes and therefore have been used to monitor the conformation and conformational change.[35−37] These conformation-dependent chemical shifts have been used for structural analyses of silk fibroins by us and other investigators.[27,28,38−40] In addition, in the ^{13}C CP/MAS NMR spectra of *B. mori* silk fibroin and related model peptides, the Ala Cβ peak becomes asymmetric and broad, and can be deconvoluted into three components reflecting the local conformation and intermolecular arrangements of the chains.[16,17] The broad component at the highest field has essentially the

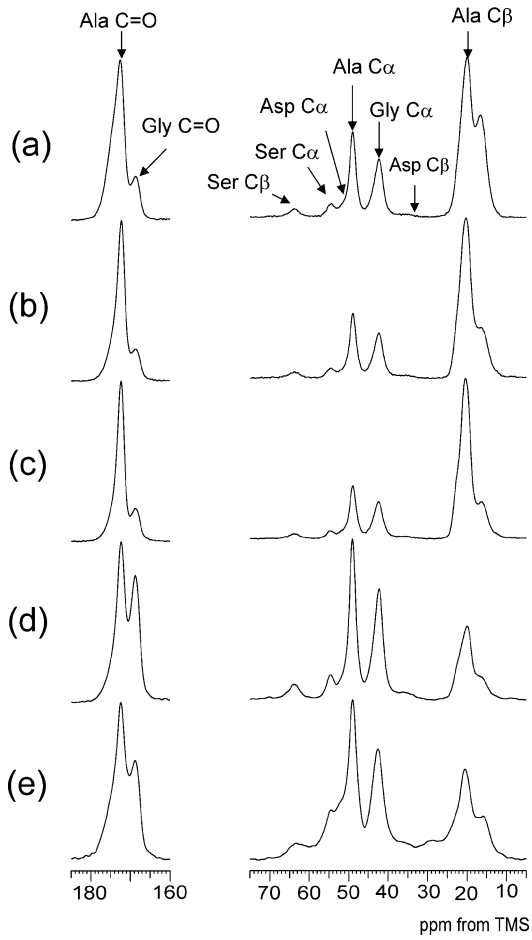

Figure 2. ^{13}C CP/MAS NMR spectra of (a) $[1\text{-}^{13}C]Ala^{12}$,$[3\text{-}^{13}C]Ala^{16}$-, (b) $[1\text{-}^{13}C]Ala^{10}$,$[3\text{-}^{13}C]Ala^{18}$-, and (c) $[1\text{-}^{13}C]Ala^{8}$,$[3\text{-}^{13}C]Ala^{20}$-labeled **41SDSDS**, (d) nonlabeled **41SDSDS**, and (e) silklike protein analogue **14DS16** together with assignments. A total of 4100−4300 scans were used for the labeled samples (a−c) and 16 300 scans for the nonlabeled samples (d and e).

Table 2. ^{13}C CP/MAS NMR Chemical Shifts (ppm from TMS) of 41SDSDS[a] and 14DS16[b] Together with the Fractions Determined for Each Deconvoluted Peak of ^{13}C-Labeled Ala Cα and C═O Carbons in the ^{13}C CP/MAS NMR Spectra of ^{13}C-Labeled 41SDSDS(Figure 4), Where the Uncertainty of the Percentages Is About ±1%

	41SDSDS							14DS16		
	(a) [1-^{13}C]A^{12},[3-^{13}C]A^{16}		(b) [1-^{13}C]A^{10},[3-^{13}C]A^{18}		(c) [1-^{13}C]A^{8},[3-^{13}C]A^{20}		(d) nonlabeled	(e) non-labeled		
carbon	ppm	fraction (%)	ppm	fraction (%)	ppm	fraction (%)	ppm	ppm	random coil[c]	silk II[c]
Ala Cβ	16.6	49	16.5	30	16.4	21	16.9	16.2	16.6	16.7
	20.1	39	20.2	48	20.3	57	20.0	20.6		19.9
	22.0	12	21.9	22	22.2	22				22.1
Ala C═O	172.6	47	172.3	67	172.4	68	172.3	172.4	175.5	172.2
	174.8	53	174.4	33	174.1	32				
Ala Cα	49.0		49.0		48.9		49.0	49.0	50.0	48.9
Gly Cα	42.3		42.3		42.4		42.3	42.6	42.9	42.5
Gly C═O	168.6		168.6		168.6		168.7	168.7	171.3	169.3
Ser Cα							54.6	54.7	55.8	54.6
Ser Cβ							63.7	63.3	61.2	63.9

[a] **41SDSDS:** $(GlyAla)_3Ser(AlaGly)_3Asp(GlyAla)_3Ser(AlaGly)_3Asp(GlyAla)_3Ser(AlaGly)_3$. [b] **14DS16:** $ThrSer[(AlaGly)_3Asp(GlyAla)_3Ser]_{16}$. [c] References 16, 17, and 27−29.

same chemical shift as the sharp Ala Cβ peak at 16.7 ppm of silk I (the solid-state structure of *B. mori* silk fibroin before spinning).[16,17] However, the corresponding structure cannot be attributed to the well-defined β-turn [type II] structure of silk I, because the diagnostic sharp peaks at 50.8 ppm (Ala Cα) and 176.8 ppm (Ala carbonyl) are missing, and instead broad lines with low intensity are observed. Therefore, we assigned the broad component at around 16.7 ppm of Ala Cβ peak to a *distorted* β-turn structure, which is characterized by a large distribution in torsion angles around an average conformation of a type II β-turn. The chemical shift of this broad peak is also in agreement with that of random coil peak of the Cβ carbon of Ala residues of proteins in aqueous solution as discussed previously.[16,17,28,37,38,41] The other two components (chemical shifts of 19.9 and 22.1 ppm) of the multicomponent Ala Cβ peak are both assigned to an antiparallel β-sheet structure, however, the methyl groups are oriented differently between the adjacent sheets. The details on the assignments have been reported previously.[16,17] The Ala carbonyl and Ala methyl peaks of (Figure 2c) [1-^{13}C]A^{8}, [3-^{13}C]A^{20}- **41SDSDS** gives information on the local conformation of Ala^{8} and Ala^{20} residues, respectively. However, there are also contributions from the corresponding carbons of the nonlabeled other Ala residues in **41SDSDS**. Therefore, we obtained the difference spectrum (c) by subtracting the natural abundance spectrum (b) from the ^{13}C-labeled peptide spectrum (a) as shown in Figure 3.[19,20] This subtraction provides exclusively local structural information for selectively ^{13}C labeled Ala residues. Figure 4 summarizes the

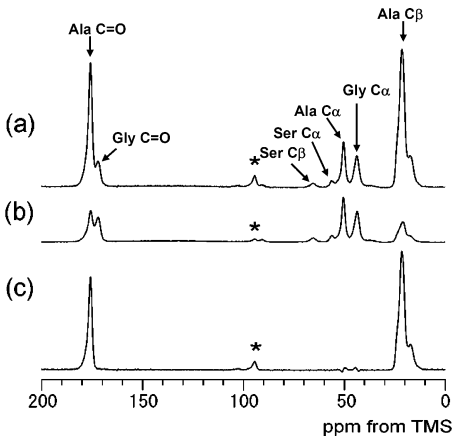

Figure 3. ^{13}C CP/MAS NMR spectra of (a) [1-^{13}C]A^{8},[3-^{13}C]A^{20}-labeled **41SDSDS** and (b) nonlabeled **41SDSDS**. The difference spectrum (c) was obtained by subtracting spectrum b from spectrum a. The asterisk means spinning side band.

difference spectra of three peptides (a−c) with different labeling positions together with the aspects of the peak decovolution assuming Gaussian distributions.[16,17] For calculation of fractions in different conformations (see Figure 4) the two peaks (20.1−20.3 and 21.9−22.2 ppm) in the Ala Cβ spectrum were summed to give the total fraction of β-sheet while peaks at 172.3−172.6 and 174.1−174.8 ppm for the Ala C═O spectra gave fractions for β-sheet and random coil respectively. The fractions determined in this way from peak deconvolution are summarized in Table 2 for the ^{13}C-labeled Ala Cβ and carbonyl carbons. The fraction of β-sheet was found to be 47% for Ala^{12} residue and 51% for Ala^{16} residue in the three ^{13}C labeled versions of **41SDSDS**. Thus, for both Ala residues located closest to the Asp^{14} residue, distorted β-turn and/or random coil accounted for half the conformations. If the Asp residue is located at the center of the turn, half of these Ala residue form β-sheet with intermolecular hydrogen bonding, but half of them take a distorted structure under the influence of the adjacent Asp residue. The high fraction of random coil strongly suggests that Asp^{14} is at the center of the turn as discussed by Wang et al.[22] for the Glu residue in the related peptide. In contrast, the fraction of β-sheet increased to 67% for Ala^{10} and 68% for Ala^{8} residues. Similarly, the β-sheet increased to 70% for Ala^{18} and 79% for Ala^{20} residue. Thus, apart from proximity to the turn position (Asp^{14}) the fraction of β-sheet was high. The fraction of β-sheet was slightly higher for Ala,^{16} Ala^{18} and Ala^{20} compared with Ala,^{12} Ala,^{10} and Ala^{8} indicating that the proportion of β-sheet slightly increased for the Ala residues located in the central parts of the stem region of the lamellar structure. As shown in Figure 2 and listed in Table 2, the Ser Cα (54.6 ppm) and Cβ (63.7 ppm) peaks indicated that the Ser residues in **41SDSDS** take almost solely a β-sheet structure.[38] The deuterium solid-state NMR study of [3,3-^{2}H$_2$]Ser *B. mori* silk fibroin fiber suggested that the hydroxyl groups of Ser interact with carbonyl groups on adjacent chains and thereby contribute to the intermolecular hydrogen-bonding network of the fiber.[26] Thus, the Ser residues in the **14DS16** may similarly contribute an additional intermolecular hydrogen bond thus further stabilizing the β-sheet structure of the stem part of **41SDSDS**. Our results from ^{13}C CP/MAS NMR indicated that there were still around 30% distorted β-turn and/or random coil in the Ala residues adjacent to the Ser residues. Parts d and e of Figure 2 show the ^{13}C CP/MAS NMR spectra of nonlabeled **41SDSDS** and **14DS16** respectively. In the latter sample the His-Tag part used to purify the protein sample was removed by cyanogen bromide cleavage. The two spectra are very similar; for example, the chemical shifts of the main peaks are identical. Thus, **14DS16** is thought

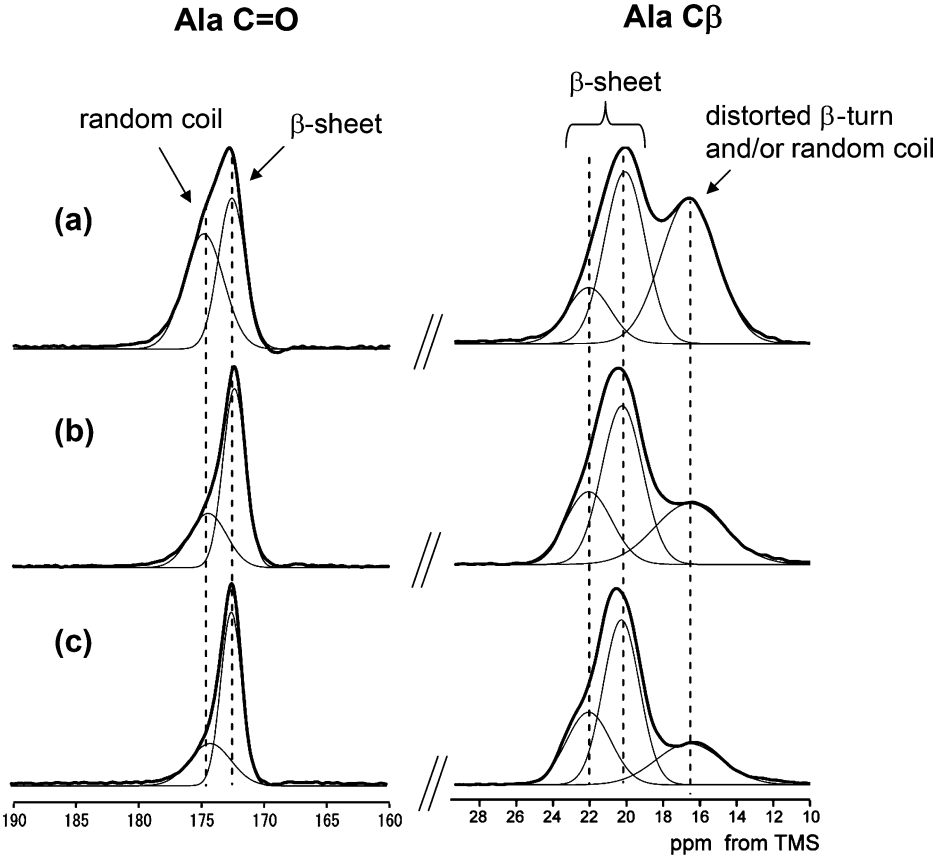

Figure 4. Expanded Ala Cβ and C═O peaks in the ^{13}C CP/MAS difference spectra of (a) [1-^{13}C]Ala^{12},[3-^{13}C]Ala^{16}-, (b) [1-^{13}C]Ala^{10},[3-^{13}C]Ala^{18}-, and (c) [1-^{13}C]Ala^{8},[3-^{13}C]Ala^{20}-labeled **41SDSDS** These spectra were obtained by subtracting the natural abundance spectrum from the ^{13}C-labeled peptide spectrum (Figure 3). Peak deconvolution was performed for each ^{13}C-labeled carbon assuming Gaussian distributions, and the fraction of each peak are summarized in Table 2. The uncertainty of the percentages is about ±1%.

to take a structure similar to that of **41SDSDS**; Asp residues are exposed on the surface of the lamellar structure and are not incorporated into the β-sheet structure.

2D Spin Diffusion ^{13}C Solid-State NMR Spectrum of 41SDSDS, [1-^{13}C]G^{15},[1-^{13}C]A^{16}-(GA)$_3$S(AG)$_3$D(GA)$_3$S(AG)$_3$D-(GA)$_3$S(AG)$_3$. ^{13}C spin diffusion NMR has been used to determine the precise structures of silk fibroins and their model peptides in the solid state through the determination of the torsion angles of the specified residues and also the fraction of each conformation where the specified residue have several conformations.[30,42] The chemical shift and peak deconvolution study of ^{13}C-labeled **41SDSDS** concluded that the Ala residue closest to the turn (Ala^{16}) takes 49% distorted β-turn and/or random coil, and 51% β-sheet structure (see above). We therefore used ^{13}C spin diffusion NMR to analyze the local structure of Ala^{16} residue in order to confirm this determination. The 2D spin-diffusion NMR spectrum of the expanded carbonyl region of [1-^{13}C]G^{15},[1-^{13}C]A^{16}-**41SDSDS** observed under off MAS conditions is shown in Figure 5a. Simulated 2D spin-diffusion spectra are shown in Figure 5b−d. The simulation assuming exclusively β-sheet structure (ϕ and $\varphi = -150°$ and $+150°$) (Figure 5c),[15] gave much weaker diagonal components than that of the observed spectrum. In contrast the simulation using exclusively the distorted β-turn and/or random coil (Figure 5d) gave more diagonal components compared with the observed spectrum. The simulated spectrum assuming values of 51% β-sheet and 49% distorted β-turn contents (determined from chemical shift and peak deconvolution of ^{13}C-labeled **41SDSDS)** (Figure 5b) was in good agreement with the observed spectrum though 2D spin-diffusion does not permit an accurate measure of the β-sheet fraction content. Thus, spin-diffusion NMR confirms our CPMAS evidence for the location of the statistical location of the turn structure centered on the Asp residue.

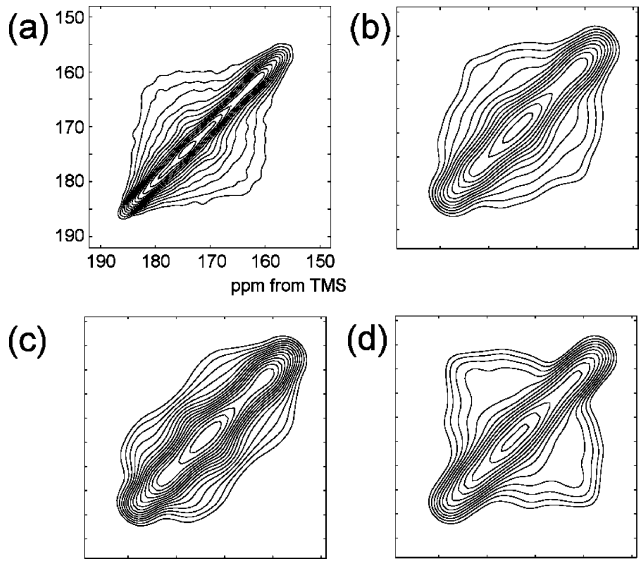

Figure 5. 2D spin diffusion ^{13}C solid-state NMR spectrum of the expanded carbonyl region of (a) [1-^{13}C]G^{15},[1-^{13}C]A^{16}-labeled **41SDS-DS** observed under off MAS condition. The simulated spectra are shown assuming (b) 51% β-sheet and 49% distorted β-turn, (c) 100% β-sheet structure (ϕ and $\varphi = -150°$ and $+150°$), and (d) 100% distorted β-turn structure and/or random coil. The method of simulation of spectrum d was reported in our previous paper.[20]

Mineralization of Films of 14DS16 in SBF. The **14DS16,** analogous to **41SDSDS** but considerably larger, was produced by genetic engineering and overexpression in *E. coli*. We

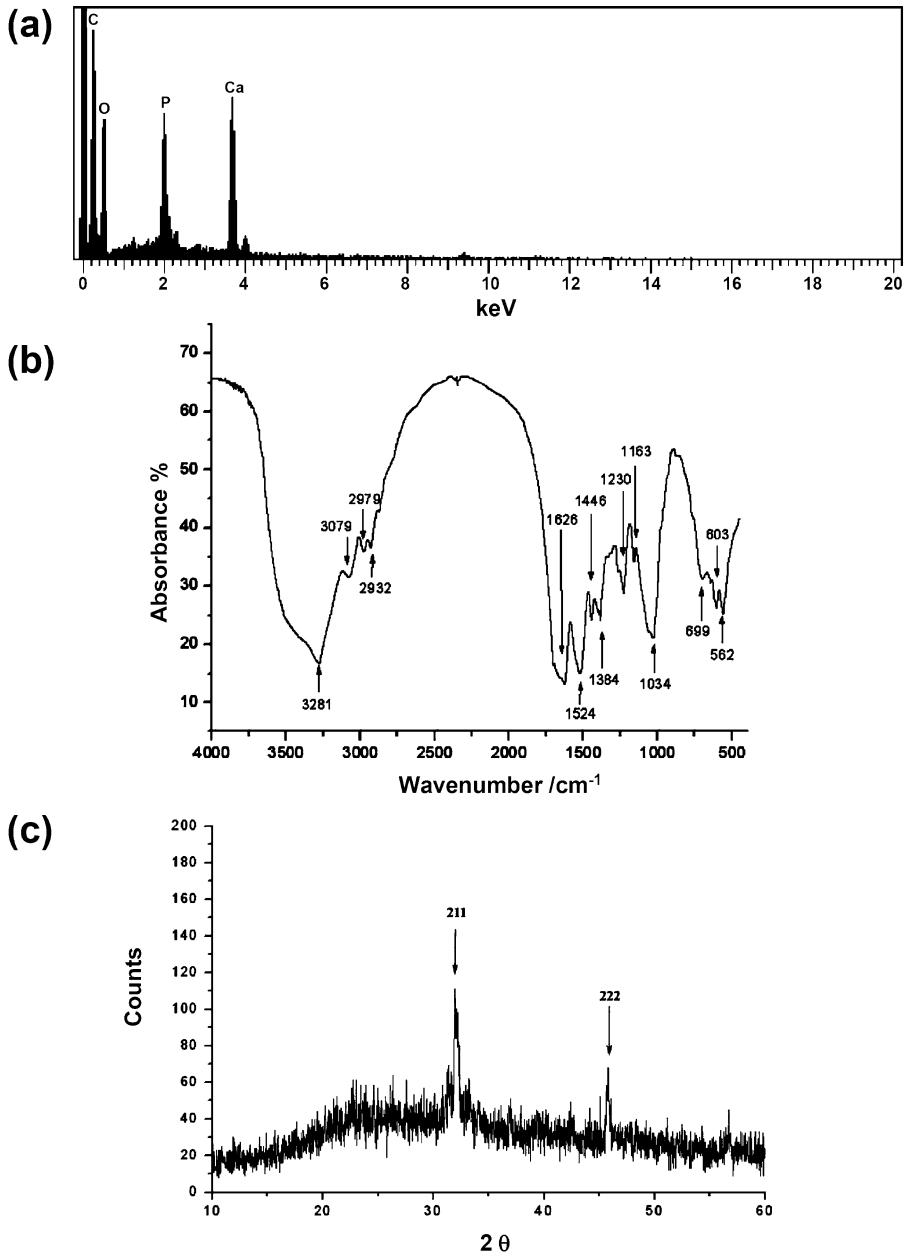

Figure 6. (a) EDX spectrum of **14DS16** film pretreated with calcium chloride and incubated in SBF for 7 days. (b) FT-IR spectrum and (c) X-ray diffractometry for the same material.

investigated the mineralization of cast films of this recombinant in simulated body fluid (SBF). An EDX spectrum of **14DS16** film pretreated with calcium chloride and incubated in SBF for 7 days showed prominent peaks for P and Ca indicating heavy mineralization with calcium phosphate (Figure 6a). An FT-IR spectrum for the same material (Figure 6b) showed prominent peaks at 562 and 603 cm^{-1} assigned to PO_4^{3-} v4 bending and at 1034 cm^{-1} assigned to asymmetric PO_4^{3-} v3 stretching. These peaks have been observed for hydroxyapatites and confirm heavy mineralization. X-ray diffractometry of the same materials (Figure 6c) gave a peak at $2\theta = 28.47$ ($d = 3.13$) assigned to the 210 plane of hydroxyapatite and a major peak at $2\theta = 2.77$ assigned to the 211 plane. A slight shoulder at $2\theta = 24.7$ ($d = 3.60$) may represent the 002 plane. Thus, X-ray diffractometry demonstrates a high level of mineralization with hydroxyapatite.

Figure 7 shows SEM micrographs of the film surfaces after 1, 3, 5, and 7 days in 1.5 SBF solution. After 1 day the surface showed no obvious sign of mineralization but after 3 days small platelike crystals were seen lying flat on the film. By day 5 the mineral appeared at low magnification as patches of a thin fairly smooth mineral coating of uniform thickness. The patches became practically confluent after 7 days suggesting a progressive growth of the mineral coating over the film. High-resolution SEMs showed that films incubated for 7 days were coated with numerous roughly spherical aggregates of platelike crystals (Figure 8, parts a and b) closely similar to those of hydroxyapatite deposited from SBF as described elsewhere.[43] Similar particles deposited at a similar density have been seen on natural silk fibroin films incubated for 7 days in SBF using a closely similar protocol.[34] In addition to the spherical aggregates, Figure 8b shows small flat mineral crystals whose epitaxial growth had clearly been defined by the surface of the film. Native fibroin is known to be capable of nucleating the formation of hydroxyapatite and controlling its epitaxial growth.[44−46] This ability may largely depend on calcium ions binding to the free carboxyl groups of the heavy chain fibroin. The published sequence of this protein[47] has 12 Asp and 8 Glu residues in the

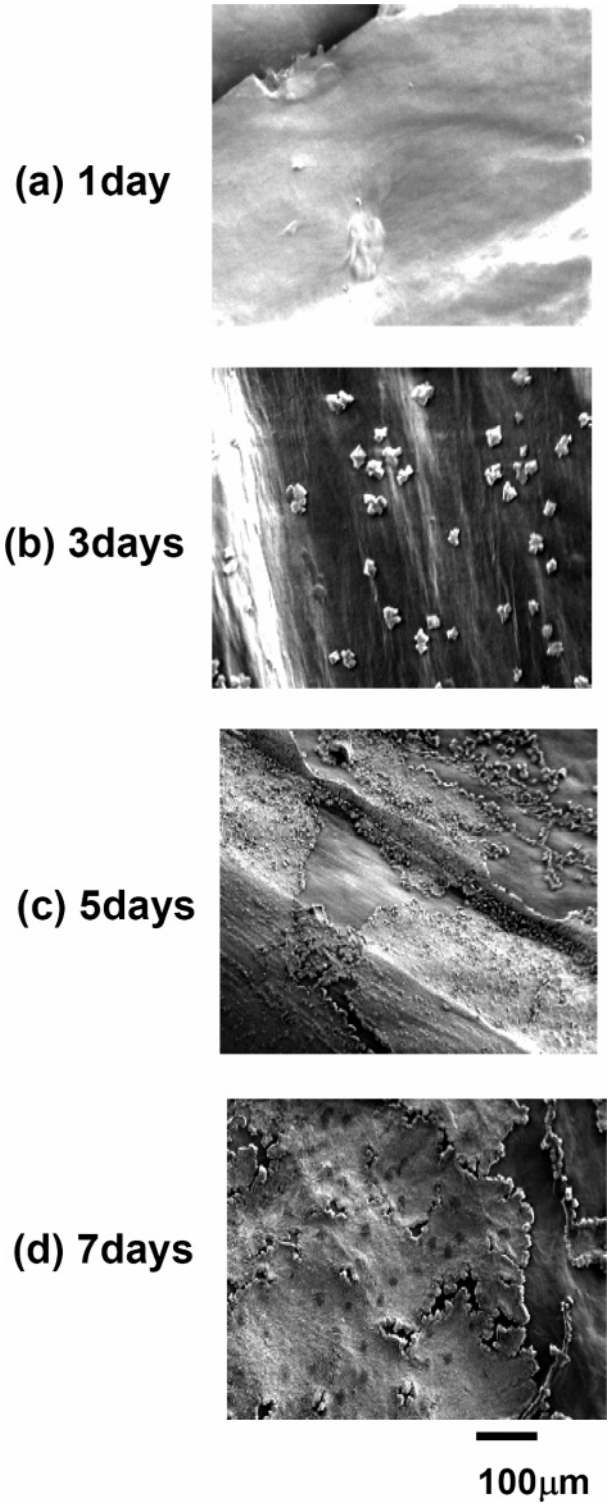

Figure 7. SEM micrographs of a film surface of **14DS16**: (a) 1, (b) 3, (c) 5, and (d) 7 days after immersing the films in SBF solution.

N-terminus and usually 1 Asp and 2 Glu residues in each of the 14 hydrophilic spacers. Thus, the hydrophilic spacers may be more important than the N-terminus in the mineralization of natural *B. mori* silk. In the case of our recombinant silklike protein it is likely that that the Asp residues located exclusively at the turn positions and exposed on the surface of the lamellar structure are responsible for calcium binding and the accelerated formation of hydroxyapatite. Our films of recombinant silklike protein clearly resemble those of native silk fibroin in their capacity for rapid and heavy mineralization in SBF.

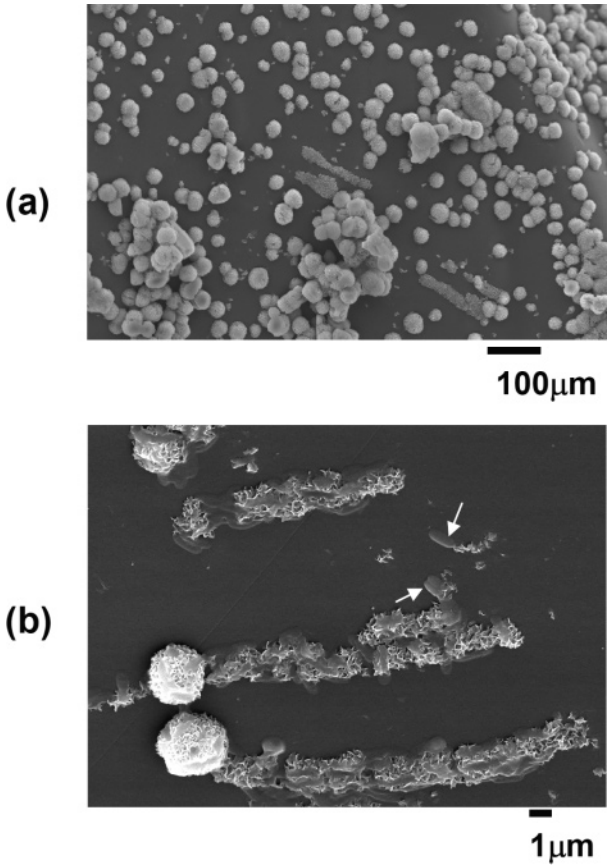

Figure 8. (a) High-resolution SEMs showing mineralization on the surface of a film of **14DS16**pretreated with calcium chloride and incubated for 7 days in SBF (Figure 7). (b) SEMs with arrows indicating small rather regular crystals with their flat surface in contact with the recombinant protein film.

Conclusions

We investigated the structure of the silklike peptide **14DS16** containing Asp as a Ca^{2+} binding site in the turn regions and Ser between $(GA)_3$ and $(AG)_3$ sequences using ^{13}C CP/MAS NMR and 2D spin diffusion ^{13}C solid-state NMR. The proportion of β-sheet evaluated by ^{13}C selective isotope labeling was high except in close proximity to the turn position Asp.[14] In addition, we showed that Ser Cα and Ser Cβ chemical shifts indicate β-sheet structure for the serine residues. Evidence from spin diffusion NMR indicated that Ala[16] was present in a mixture of distorted β-turn and β-sheets. Together these observation provide strong evidence for a lamellar structure in which the $(GA)_3S(AG)_3$ motifs form the stem of the lamella mainly in the β-sheet conformation while the Asp residues are present in the turn region and not in the stems. The silklike protein analogue, **14DS16** designed on the basis of our structural analysis of **41SDSDS** was rapidly and heavily mineralized in SBF solution and may have potential for use in implantable biomaterials, particularly as a bone graft substitute or in other applications where mineralization is important.

Acknowledgment. T.A. acknowledges Dr. Hajime Saito for stimulating discussions. Dr. Jun Ashida (Varian Technologies Japan) is also acknowledged for his useful suggestions about solid-state NMR measurements. T.A. also acknowledges support from a Grant-in-Aid for Scientific Research from the Ministry of Education, Science, Culture, and Sports of Japan (18105007). D.K. and A.M.C. acknowledge support from the EU FP6 SilkBone project grant and help and advice from Prof. Stephen Mann.

References and Notes

(1) Shao, Z.; Vollrath, F. *Nature* **2002**, *418*, 741.
(2) Gillespie, D. B.; Viney, C.; Yager, P. In *Silk Polymers, Material Science and Technology*; Kaplan, D., Adams, W. W. F., Farmer, B., Viney, C., Eds.; ACS Symposium Series: Washington, DC, 1994; pp 155−167.
(3) Sinsawat, A.; Putthanarat, S.; Magoshi, Y.; Pachter, R.; Eby, R. K. *Polymer* **2002**, *43*, 1323−1330.
(4) Altman, G. H.; Diaz, F.; Jakuba, C.; Calabro, T.; Horan, R. L.; Chen, J.; Lu, H.; Richmond, J.; Kaplan, D. L. *Biomaterials* **2003**, *24*, 401−416.
(5) Vincent, J. F. V. *Biomechanics Materials: A Practical Approach*; Oxford University Press: Oxford, U.K., 1992.
(6) Miranda, D. A. O.; Blumenthal, N. M.; Sorensen, R. G.; Wozney, J. M.; Wikesjö, U. M. E. *J. Periodontology* **2005**, *76*, 210−220.
(7) Dal, Pra, I.; Chiarini, A.; Bochi, A.; Freddi, G.; Armato, U. *Int. J. Mol. Med.* **2006**, *18*, 241−247.
(8) Li, C. M.; Vepari, C.; Jin, H. J.; Kim, H. J.; Kaplan, D. L. *Biomaterials* **2006**, *27*, 3115−3124.
(9) Meinel, L.; Betz, O.; Fajardo, R.; Hofman, S.; Nazarian, A.; Cory, E.; Hilbe, M.; Mccool, J.; Ranger, R.; Novakonic, V. G.; Merkle, P.; Rechenberg, B.; Kaplan, D. L.; K-Head, C. *Bone* **2006**, *39*, 922−931.
(10) Nazarov, R.; Jin, H. J.; Kaplan, D. L. *Biomacromolecules* **2004**, *5*, 718−726.
(11) Wang, Y. Z.; Blasioli, D. J.; Kim. H. J.; Kim, H. S.; Kaplan, D. L. *Biomaterials* **2006**, *27*, 4434−4442.
(12) Wang, Y. Z.; Kim, H. J.; Novakovic, V. G.; Kaplan, D. L. *Biomaterials* **2006**, *27*, 6064−6082.
(13) Marsh, R. E.; Corey, R. B.; Pauling, L. *Biochim. Biophys. Acta* **1955**, *16*, 1−34.
(14) Takahashi, Y.; Gehoh, M.; Yuzuriha, K. *Int. J. Biol. Macromol.* **1999**, *24*, 127−138.
(15) Demura, M.; Minami, M.; Asakura, T.; Cross, T. A. *J. Am. Chem. Soc.* **1998**, *120*, 1300−1308.
(16) Asakura, T.; Yao, J.; Yamane, T.; Umemura, K.; Ulrich, A. S. *J. Am. Chem. Soc.* **2002**, *124*, 8794−8795.
(17) Asakura, T.; Yao, J. *Protein Sci.* **2002**, *11*, 2706−2713.
(18) Panitch, A.; Matsuki, K.; Cantor, E. J.; Cooper, S. J.; Atkins, E. D. T.; Fournier, M. J.; Mason, T. L.; Tirrel, D. A. *Macromolecules* **1997**, *30*, 42−49.
(19) Asakura, T.; Nakazawa, Y.; Ohnishi, E.; Moro, F. *Protein Sci.* **2005**, *14*, 2654−2657.
(20) Asakura, T.; Sato, H.; Moro, F.; Nakazawa, Y.; Aoki, A. *J. Am. Chem. Soc.* **2007**, *129*, 5703−5709.
(21) van Hest, J. C. M.; Tirrell, D. A. *Chem. Commun.* **2001**, 1897−1904.
(22) Wang, J.; Parkhe, A. D.; Tirrel, D. A.; Thompson, L. K. *Macromolecules* **1996**, *29*, 1548−1553.
(23) Parkhe, A. D.; Cooper, S. J.; Atkins, E. D. T.; Fournier, M. J.; Mason, T. L.; Tirrell, D. A. *Int. J. Biol. Macromol.* **1998**, *23*, 251−258.
(24) Sudo, S.; Fujikawa, T.; Nagakura, T.; Ohkubo, T.; Sakaguchi, K.; Tanaka, M.; Nakashima, M. *Nature* **1997**, *387*, 563−564.
(25) Asakura, T.; Hamada, M.,; Ha, S.-W.; Knight, D. *Biomacromolecules* **2006**, *7*, 1996−2002.
(26) Kameda, T.; Ohkawa, Y.; Yoshizawa, K.; Naito, J.; Ulrich, A. S.; Asakura, T. *Macromolecules* **1999**, *32*, 7166−7171.
(27) Asakura, T.; Sugino, R.; Yao, J.; Takashima, H.; Kishore, R. *Biochemistry* **2002**, *41*, 4415−4424.
(28) Zhao, C.; Asakura, T. *Prog. Nucl. Magn. Spectrosc.* **2001**, *39*, 301−315.
(29) Harris, R. K.; Becker, E. D.; Cabral de Menezes, S. M.; Granger, P.; Hoffman, R. E.; Zilm, K. W. Further conventions for NMR Chemical Shifts (IUPAC Recommendations 2006), December 21, 2006.
(30) Asakura, T.; Ashida, J.; Yamane, T.; Kameda, T.; Nakazawa, Y.; Ohgo, K.; Komatsu, K. *J. Mol. Biol.* **2001**, *306*, 291−305.
(31) Yao, J.; Yanagisawa, S.; Asakura, T. *J. Biochem.* **2004**, *136*, 643−649.
(32) Asakura, T.; Tanaka, C.; Yang, M.; Yao, J.; Kurolawa, M.; Takahashi, Y. *Biomaterials* **2004**, *25*, 617−624.
(33) Yang, M.; Asakura, T. *J. Biochem.* **2005**, *137*, 721−729.
(34) Kino, R.; Ikoma, T.; Monkawa, A.; Yunoki, S.; Munekata, M.; Tanaka, J.; Asakura, T. *J. Appl. Polym. Sci.* **2006**, *99*, 2822−2830.
(35) Saito, H. *Magn. Reson. Chem.* **1986**, *24*, 835−852.
(36) Spera, S.; Bax, A. *J. Am. Chem. Soc.* **1991**, *113*, 5490−5492.
(37) Iwadate, M.; Asakura, T.; Williamson, M. P. *J. Biomol. NMR.* **1999**, *13*, 199−211.
(38) Asakura, T.; Iwadate, M.; Demura, M.; Williamson, M. P. *Int. J. Biol. Macromol.* **1999**, *24*, 167−171.
(39) Simmons, A. H.; Michal, C. A.; Jelinski, L. W. *Science* **1996**, *271*, 84−87.
(40) Liivak, O.; Flores, A.; Lewis, R.; Jelinski, L. W. *Macromolecules* **1997**, *30*, 7127−7130.
(41) Asakura, T.; Watanabe, Y.; Uchida, A.; Minagawa, H. *Macromolecules* **1984**, *17*, 1075−1081.
(42) Kummerlen, J.; van Beek, J. D.; Vollrath, F.; Meier, B. H. *Macromolecules* **1996**, *29*, 2920−2928.
(43) Ohta, K.; Kikuchi,; Tanaka, J. *Bioceramics* **2004**, *16 254−2*, 15−18.
(44) Nemoto, R.; Nakamura, S.; Isobe, T;, Senna, M. *J. Sol-Gel Sci. Technol.* **2001**, *21*, 7−12.
(45) Kong, X. D.; Cui, F. Z.; Wang, X. M.; Zhang, M.; Zhang, W. *J. Cryst. Growth* **2004**, *270*, 197−202.
(46) Wang, L.; Nemoto, R.; Senna, M. *J. Eur. Ceram. Soc.* **2004**, *24*, 2707−2715.
(47) Tsujimoto, Y.; Suzuki, Y. *Cell* **1979**, *18*, 591−600.

MA0713759